Sensors & Actuators: A. Physical 377 (2024) 115739

Contents lists available at ScienceDirect

Sensors and Actuators: A. Physical

journal homepage: www.journals.elsevier.com/sensors-and-actuators-a-physical

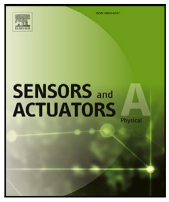

Experimental hot-wire characterisation of the turbulent jet produced by a sweeping jet actuator in a quiescent environment

Mathieu Tocquer *, Cédric Raibaudo, Azeddine Kourta

Université d'Orléans, INSA-CVL, PRISME, EA 4229, 8 rue Léonard de Vinci, Orléans, F45072, France

ARTICLE INFO

Keywords:
Sweeping jet
Experimental
Compressible flow
Flow control

ABSTRACT

The present work presents the design and the characterisation of a sweeping jet, a fluidic actuator that has been shown to be able to enhance the aerodynamic performance of flow applications as transportation vehicles. The principles and operation of this type of actuator are detailed here. An experimental apparatus with hot-wire anemometry was installed to describe the flow topology produced by the sweeping jet. Basic analysis shows that the jet generates a flow with an average velocity of $60 < U_{mean} < 100$ ms^{-1}, a flow rate between 1.3 and 3 gs^{-1}, and an oscillating frequency up to 2200 Hz. The produced jet geometry is also analysed and shows interesting behaviour. The evolution of geometrical parameters is influenced by a transonic transition inside the actuator. To analyse the turbulent properties of the external flow, spectral triple decomposition is developed and used on the experimental data. A strong impact of the transition from a subsonic to a transonic regime on the produced flow is highlighted. The analysis of the turbulence produced by the sweeping jet shows a separation of the flow in three different zones detailed in the article. The study highlights promising results for future flow control implementations.

1. Introduction

In the present environmental context, the reduction of CO_2 emissions from vehicles is of primary importance. As an example, as presented by the Official Airline Guide (OAG) in 2022 [1], for a relatively short flight distance (London–Paris), up to 20% of the fuel is consumed during the plane take-off and landing (see Fig. 1). During those flight phases, planes need to have a high angle of attack in order to shorten the time of landing and increase the rate of takeoff at the airport. But wings are not tuned for those phases and can exhibit turbulent separations, which can lead to the stall of the plane or an increase in aerodynamic drag.

Thus, for takeoff and landing, aerodynamic performances need to be enhanced. Possibilities exist. Among them, the change of the geometry of the wings to have a better aerodynamic shape. For example, during the take-off, the plane struggles to have sufficient lift at a high angle of attack. The current solution is to modify the geometry of the wings by installing flaps and slats on the trailing edge and the leading edge of the wings to increase the lift at high angles of attack. This solution a has limited efficiency range and also leads to an important increase in drag and the total weight of the plane, which generates a significant rise in energy consumption.

The other solution is to directly influence the flow to improve aerodynamic performances. Passive control has been used in the past to energise the boundary layer before the separation point, using additional roughness [2], riblets, or passive vortex generators [3]. This technique is really efficient for designed flow conditions, such as during takeoff, but can lead to side effects for other flow conditions by creating additional drag during a cruise flight, for example. Another approach is to use active flow control, which is therefore capable of adapting to the flight conditions and being deactivated during the cruise phase. Active flow control actuators have been used in the past: fluidic jets (steady [4], pulsed [5]), synthetic jets [6–8], fluidic oscillators [9], DBD plasma actuators [10], etc. The objective is mostly to reach significant momentum injection and high frequency ranges for unsteady actuators [11], which are not always possible for actuators detailed previously.

Fig. 2 presents many actuators used in the past and compares them in terms of frequency and maximum produced velocity. It is shown that for automotive applications, actuators need to reach moderate velocity (between 10 and 100 m s^{-1}) and moderate frequency (between 50 and 1000 Hz). However, to control flow on aeronautic devices the velocity and the frequency of the produced jet need to be high (respectively between 80 and 800 m s^{-1} and between 500 and 10 000 Hz).

* Corresponding author.
E-mail addresses: mathieu.tocquer@univ-orleans.fr (M. Tocquer), cedric.raibaudo@univ-orleans.fr (C. Raibaudo), azeddine.kourta@univ-orleans.fr (A. Kourta).

https://doi.org/10.1016/j.sna.2024.115739
Received 6 May 2024; Received in revised form 4 July 2024; Accepted 22 July 2024
Available online 25 July 2024

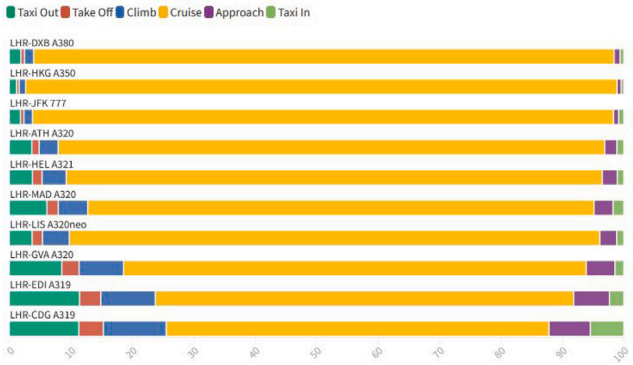

Fig. 1. Estimated fuel burn by flight stage for different aircraft and cruise distance. Top corresponds to the highest flight distance and bottom to the lowest. Taken for Official Airline Guide OAG [1].

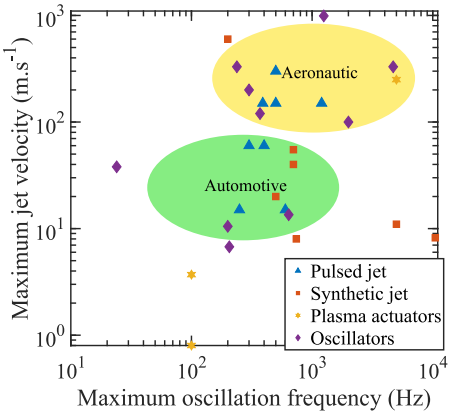

Fig. 2. State of art of different fluidic actuators used in flow control applications. Results for pulsed jets are taken from [12–19]. Results for synthetic jets are taken from [6,8,20–24]. Results for plasma actuators are taken from [25–27]. Results for oscillators are taken from [28–37].

Among all the active control actuators, the sweeping jet (SWJ) in particular has attracted a lot of attention in recent years. The latter is able to produce high momentum injection and high frequency oscillation using no moving part and only pressure injection [38,39]. To produce the sweeping motion, the periodic mechanism used by the sweeping jet can be decomposed in three steps. Those steps are presented in Fig. 3. First, the flow at the inlet nozzle attaches to one of the main chamber surfaces due to the Coanda effect. The flow at the outlet is then deflected in the opposite direction (Fig. 3a). Then, a part of the main flow enters inside the feedback loop and begins to create a recirculation at the entrance of the sweeping jet (Fig. 3b). This recirculation continues to grow until it pushes the main flow onto the other surface of the main chamber. During the internal shift, the flow at the outlet is deviated in the other direction (Fig. 3c). And so on.

Previous works studied the influence of the inlet pressure or the flow rate on the oscillation frequency generated by the sweeping jet [30,40,41]. The oscillation frequency f_{osc} was found to be linear with respect to the inlet pressure P_0 for lower pressures. It corresponds to an incompressible phase inside the SWJ. For higher pressures, the oscillation frequency reaches a plateau corresponding to the compressible state inside the SWJ. The sweeping jet is an active flow control device that injects periodic high-momentum fluid into the surface's boundary layer. The jet is angled in such a way that it sweeps across the surface, inducing a span-wise vorticity and adding momentum in the boundary layer that can enhance mixing and thus reduce flow separation. Sweeping jets can be used in a wide variety of flow control applications. For instance, they have been applied to enhance the

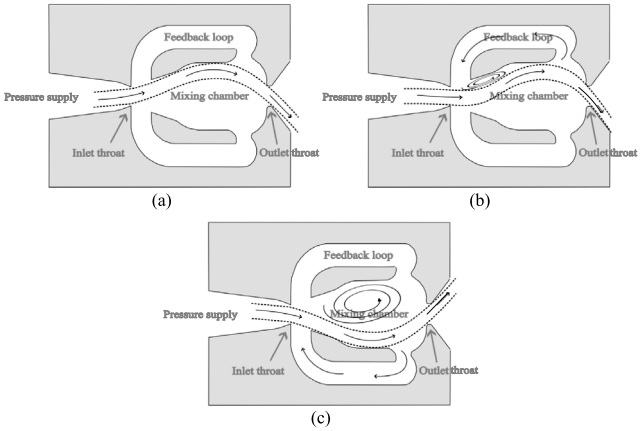

Fig. 3. Working principle of the sweeping jet actuator. (a),(b) and (c) Different phases of the sweeping phenomena.

performance of aircraft wings [31,32,42], land vehicles [33,34] and even underwater vehicles [35]. Sweeping jets have also been used to reduce negative effects of flow separation, like noise and vibration [40]. The understanding of sweeping jets and their potential for flow control has, however, significantly advanced as a result of recent developments in experimental and computational methodologies [30,36,37].

In the objective of flow control with the sweeping jet, an exhaustive comprehension of the interaction between the main flow and the sweeping jet is needed. The latter will interact with a turbulent boundary layer and influence a turbulent separation, which exhibits unsteady behaviour at relatively high frequencies. In addition, despite the potential benefits of sweeping jets, the underlying fluid mechanics of the device are still not well understood. As a result, designing and refining sweeping jets for particular flow control applications remains a challenge. In their study Tajik et al. [43] show the effect of slight changes on the internal geometry on the produced flow using hot-wire measurement. They have highlighted two types of SWJs: the bifurcated and the homogeneous SWJs, showing different dynamic and geometric properties on the produced flow. An exhaustive understanding of the flow dynamics generated by the jet is therefore necessary for the implementation of these actuators for flow control. In the present study, the actuators have been characterised, especially on important parameters for control application such as the oscillation frequency and the jet geometry. The turbulence produced by the sweeping jet is also studied. To do so, hot wire measurements are used, and the experimental set-up as well as the geometry of the sweeping jet characterised in this work are presented in Section 2. Then, in the next Section 3, the evolution of the dynamics of the jet as well as the geometry of the latter is explored. The impact of the transonic transition on those parameters is highlighted. A triple decomposition based on a spectral analysis is also developed in order to study the turbulence produced by the sweeping jet. Three different zones are emphasised. Finally, a conclusion on the present work is given, and some future work perspectives are presented in Section 4.

2. Experimental set-up

Experimental facility. Experiments were conducted in the Flow Control Actuators experimental platform of the PRISME Laboratory at Orléans, France. The platform used in this study is the same as [44]. The platform consists of three ISEL displacement robots which can be controlled in position with a precision of 0.1 mm. It allows to cover a large spatial range to study the expansion of the jet wake. A 55P11 hot-wire probe is fixed on the platform in order to measure(d) the velocity of the flow produced by the sweeping jet. Stream Ware software is used to control the position of the hot-wire and the acquisition of velocity

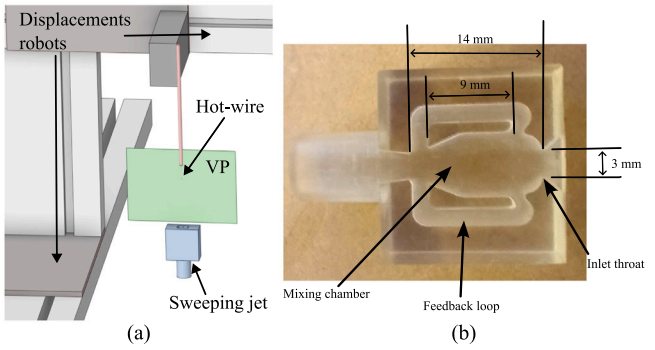

Fig. 4. Experimental set-up. (a) Platform used for the actuator characterisation. (b) Dimension of the actuator.

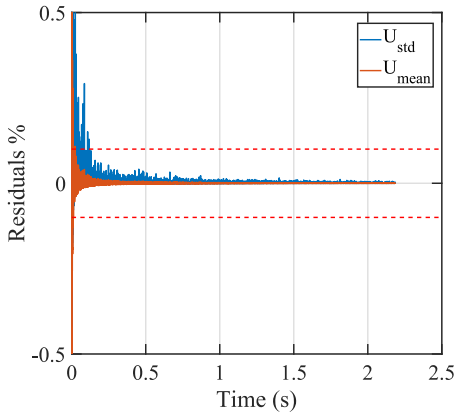

Fig. 5. Convergence of U_{mean} and U_{std} for hot-wire measurement. P_0 = 20 kPa. Horizontal red dotted lines represent the convergence threshold of 0.1%.

data. Acquisition parameters are detailed below. The sweeping jet is connected to a manometer to measure the inlet pressure P_0. The total flow rate Q is measured using a flowmeter upstream the valve. The experimental-setup is presented in Fig. 4a.

Sweeping jet geometry. The sweeping jet shape used for this study is presented in Fig. 4b. The actuator has been 3D printed using a Fromlabs Form 2 SLA 3D printer with a resolution of 25 µm. The actuator used here consists of a main chamber connected to the pressure supply through a nozzle of width 3 mm. The end of this chamber has three outputs: the main outlet and two feedback paths of 9 mm length, allowing part of the main flow to recirculate. The throat to throat length of the actuator is L_{osc} = 14 mm. The throat height of the sweeping jet is H = 3 mm and is used for normalisation of the main geometrical parameters and other variables in the following.

Metrology and flow conditions. To characterise the flow produced by the jet, hot-wire anemometry (HWA) is performed. A 55P11 single-component hot-wire sensor from DANTEC is set to the ISEL displacement system. The total velocity $U_{tot} = \sqrt{U^2 + V^2 + W^2}$ is measured from this 1D sensor. The sensor is moved downstream the jet exit in the generated flow, the measurement plan is then presented in Fig. 4a. It corresponds to a vertical plan (VP) at the middle of the jet. The range of interest is $15H \times 20H$ with $\frac{1}{6}H \leq \Delta_{Y,Z} \leq 1H$. The sampling frequency is F_s = 60 kHz and the acquisition time T_s = 2 s for each spatial position, corresponding to at least 1000 periods of oscillation for the lowest oscillation frequency tested.

The sensor is calibrated for every tested pressure using a turbulent round jet produced by TSI Model 1125 hot-wire anemometry calibrator with an exit nozzle of 4 mm diameter. The calibration is performed using 20 inlet velocities, in the range of Mach number between 0 to 0.9, corresponding to a jet velocity range between 0 and 300 m s^{-1}. A fourth order polynomial interpolation is then applied as standard calibration law [45]. Nine relative inlet pressure P_0 are tested in this work from 20 kPa to 100 kPa. To estimate the oscillation frequency (presented in next section), only one point measurement is needed. Therefore for a better characterisation of the dynamic of the sweeping jet, a wider range of pressure, from 2 kPa to 100 kPa, is used to estimate the oscillation frequency f_{osc}. The nine tested pressures corresponds to a flow rate from $0.9e^{-3}$ to $1.3e^{-3}$ m^3 s^{-1} (or 1.3 to 3 g s^{-1}). The inlet velocity U_{ref} is estimated from this flow rate and is used as reference velocity value for normalisation of the variables in this paper.

Quality of measurements. The uncertainties on the velocity are estimated by averaging the error of the calibration on three different speeds in the range of the calibration. The error for all calibration is less than 2%. The inlet pressure is collected with an electronic manometer with a precision of 300 Pa. The flow rate is acquired using the BROOK 5853E flowmeter with a precision of $8.3e^{-5}$ m^3 s^{-1}. For all velocity measurements the convergence is checked and residuals for the mean and the standard deviation of the worst case are presented in Fig. 5.

This measure corresponds to Y/H = 4, Z/H = 6.5 and an inlet pressure of 20 kPa. Residuals are estimated using:

$$Residuals = \frac{(u^n_{mean/std} - u^{n-1}_{mean/std})}{u_{mean/std}} \quad (1)$$

where $u^n_{mean/std}$ corresponding to the mean and standard deviation using only the n first values of the signal. The mean velocity is converged at less than 0.1% really quickly (for $t > 0.02$ s). For the standard deviation the convergence is achieved latter for $t > 0.12$ s.

3. Physics of the sweeping jet

The main results of the experimental characterisation of the sweeping jet are presented in this section. The jet is studied through different aspects: (a) the main oscillation frequency generated, (b) the mean wake topology properties and (c) a triple decomposition to extract the turbulence components.

Oscillation frequency. As presented in the introduction, the unsteady sweeping jet is oscillating around a main oscillation frequency f_{osc}. The oscillation frequency with respect to the inlet pressure is presented in Fig. 6. A linear trend of the oscillation frequency (Fig. 6a) can be observed for $P_0 \leq$ 10 kPa. For higher pressures, the oscillation frequency reaches a maximum in the range of pressure studied in this paper. Compared to similar fluidic oscillators, sweeping jet can achieve higher frequencies with the same (momentum coefficient). For example, the frequency is multiplied by up to 4 compared to a fluidic oscillator using Coanda effect [29] (see Fig. 6). For a better comparison between different sweeping jet geometries, the oscillation frequency is scaled as a convective velocity and the convective Mach number M_{conv} (Eq. (A.2)) is calculated and presented in Fig. 6b, with respect to the inlet Mach number M_{jet} estimated from the inlet pressure using isentropic laws (Eq. (A.3)). Detailed calculation method for the convective Mach number M_{conv} is presented in Appendix.

A linear trend found by Schmidt et al. [35] is also observed in this study for the incompressible tested cases ($P_0 <$ 10 kPa), but the slope of the linear relation is steeper in this experiment. For higher inlet pressure ($P_0 \geq$ 15 kPa), the flow becomes compressible and the evolution of the convective Mach number deviate from the linear trend for $M_{jet} \geq 0.8$ showing a transition on the behaviour of the jet. This fits with the findings of Hirsch and Gharib [37] for compressible sweeping jets. Despite the non linear evolution found in this study, the present results differs from the one of Hirsch and Gharib for compressible tested cases. This could be explained by the use tetrafluoroethane gas in their

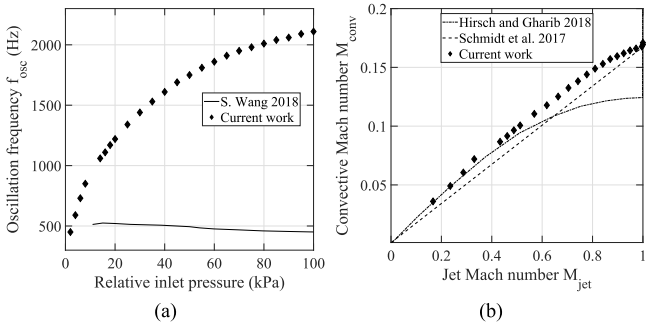

Fig. 6. Oscillation frequency of the sweeping jets. (a) Oscillation frequency with respect to the inlet pressure. (b) Convective Mach number with respect to the Mach number at the outlet throat M_{jet} respectively defined in Eqs. (A.2) and (A.3).

study. Nevertheless, the correlation between the convective and the jet Mach number shows that the oscillatory behaviour of the sweeping jet is highly dependent of its geometry, especially the throat to throat length L_{osc} (Eq. (A.2)). During the transition from incompressible to compressible flow, the SWJ stops its oscillatory behaviour as seen in Fig. 6 for $10 \leq P_0 \leq 13$ kPa and $0.32 \leq M_{jet} \leq 0.41$.

Mean wake topology. Maps of the mean velocity measured by HWA in the vertical plane (VP) are presented in Fig. 7, for different inlet pressures.

Parts of the velocity maps are missing, especially for the highest inlet pressures, due to high velocities generated by the actuators that could break the sensor. In those regions, the instantaneous flow produced by the SWJ can reach a velocity of more than 300 m s^{-1}, which creates high constraint on the hot-wire and leads to its failure. However, this lack of data for high pressure only impact the estimation of the shape coefficient S (define in the next paragraph). The error on this parameter depending on the proportion of flow captured is estimated on the 20 kPa and 30 kPa cases. When the measured flow captured more than 30% of the jet height, the error on S is less than 3.5%. Knowing that in the worst case, 34% of the jet height is captured ($P_0 = 90$ kPa). Even if it is not considered in this work, reconstruction or clustering technics could be employed to reduce the uncertainty inferred by the missing part of velocity data for high inlet pressure. In this goal, clustering technic based on fuzziness approach can be employed [46,47]. By adding additional sensors, data-driven CFD simulations can also be employed to estimate the missing part of data by constraining the simulations with the existent experimental measurements [48,49]. Dots on the figure correspond to the maximum of velocity for the left and right sides of the jet, indicating therefore the jet angles.

A butterfly shape can be observed. This particular shape informs us, qualitatively, on the residence time of the jet inside the actuator. The presence of high velocity regions at both sides of the jet shows that the jet spends more time on sides of the mixing chamber of the SWJ for each period of oscillation (Fig. 3). It corresponds to the conclusions of Koklu et al. [36], conducted only in the linear range of the oscillation frequency (compressible flow inside the actuator). Here, the result is extended to the incompressible flows. For high inlet pressures the shape of the jet becomes more homogeneous hinting on a change in the internal switching mechanism. However, as presented by [43,50] recently, slight changes in the internal geometry or surface roughness can lead to important changes on the flow generated by the jet.

To quantify the geometrical properties of the flow shape, the mean wake is delimited using a threshold. It corresponds to the half of the reference velocity U_{ref} defined in Section 2, based on a criterion defined by Ostermann et al. [30].

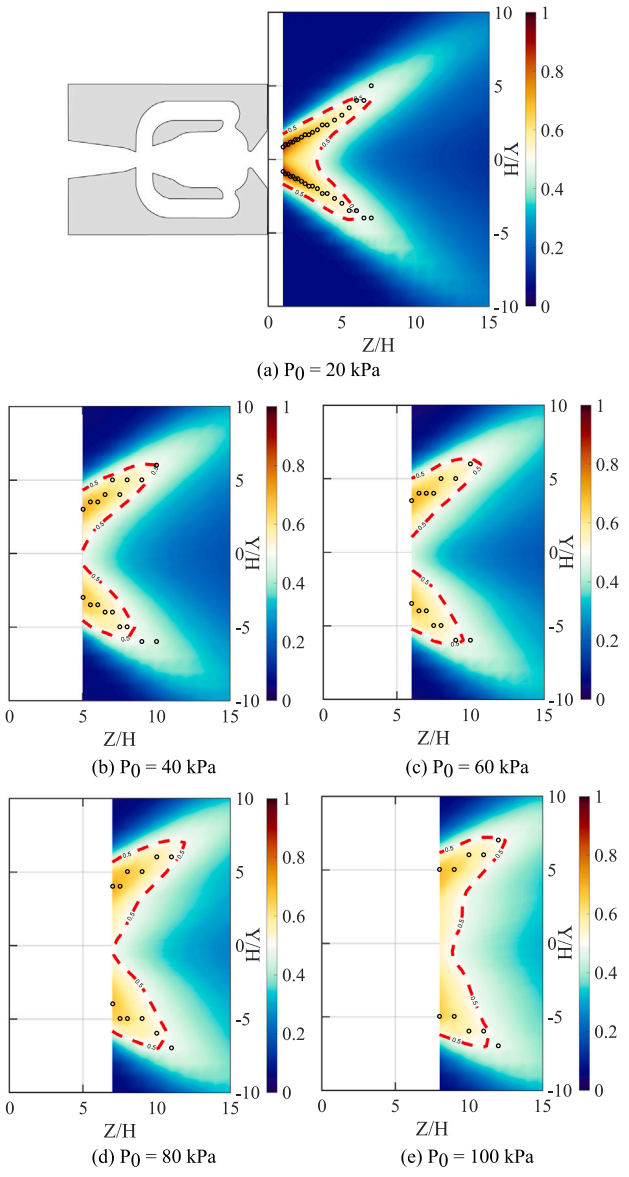

Fig. 7. Mapping of the dimensionless mean velocity (U_{mean}/U_{ref}). (– –) : Jet detection threshold ($U = 0.5U_{ref}$). (°) : Maximum right/left of the mean velocity.

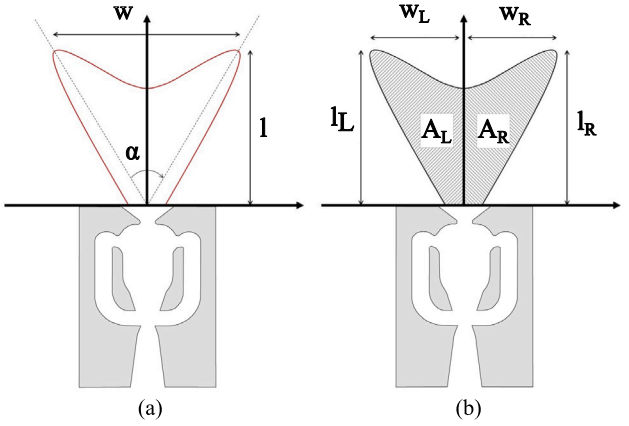

Fig. 8. Definition of the geometrical variables. (a) Variables used for the general geometry of the jet. (b) Variables used for the symmetry of the jet.

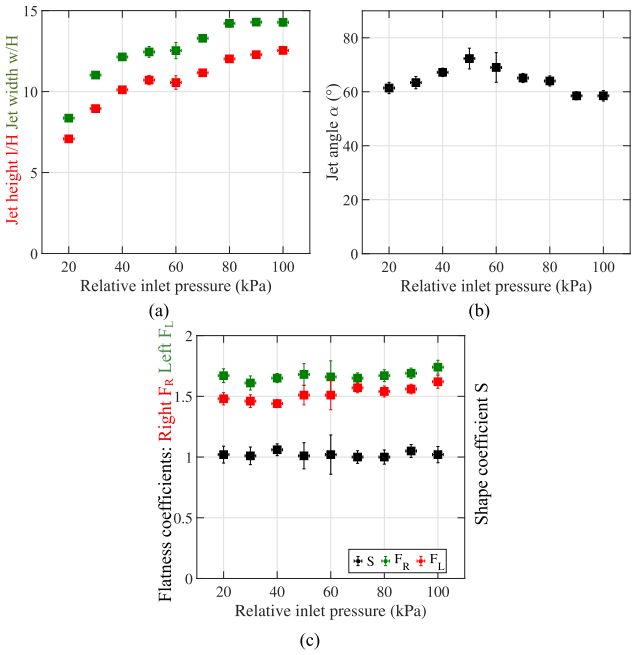

Fig. 9. Evolution of geometric parameters of the jet produced by the SWJ. (a) Evolution of the height and the width of the jet. (b) Evolution of the jet angle. (c) Shape symmetry. S : Shape coefficient, F_R : Right flatness and F_L : Left flatness.

Geometrical parameters of the jet. From the mean shape detected with the threshold defined in the previous section, geometric variables are estimated for quantification.

The shape is defined by three parameters presented in Fig. 8a: the height l defined as the maximum height of the threshold contour, the width w corresponding to the total width of the contour and the jet angle α.

The jet symmetry is also studied here, using three coefficients. The first one is the shape coefficient S, defined as:

$$S = \frac{2A_R}{A_R + A_L} \tag{2}$$

With A_R the area of the right part, and A_L the area of the left part. The other two coefficients represent the flatness of the right and the left parts, defined as:

$$F_{L,R} = \frac{l_{L,R}}{w_{L,R}} \tag{3}$$

With l and w respectively the length and the width where indexes R and L represent the side considered. The definition of these coefficients is illustrated in Fig. 8b. The jet is considered symmetric when the area of the right and left part are equal ($S = 1$) and when the flatness of the right part is the same as the left part ($F_R = F_L$).

The evolution of the geometrical parameters described previously is detailed in Fig. 9. For the height and width (Fig. 9a), a continuous increase is observed at low and high inlet pressures, with a break in the evolution for an inlet pressure around 60 kPa corresponding to the transition found for $M_{jet} \geq 0.8$. The width reaches a plateau at 14H for high pressure.

The jet angle is presented in Fig. 9b. A similar break between 50 kPa and 60 kPa is also visible in the jet angle. It increases from 60° to 70°, reaches a maximum at 50 kPa, then decreases down to 60° for high inlet pressures.

An explanation for the abrupt change of trend of w, l and α would be a change of the flow regime. Using isentropic laws, this pressure of 50 kPa corresponds to a Mach number at the inlet throat of $M = 0.8$, corresponding to the flow becoming transonic. In order to confirm

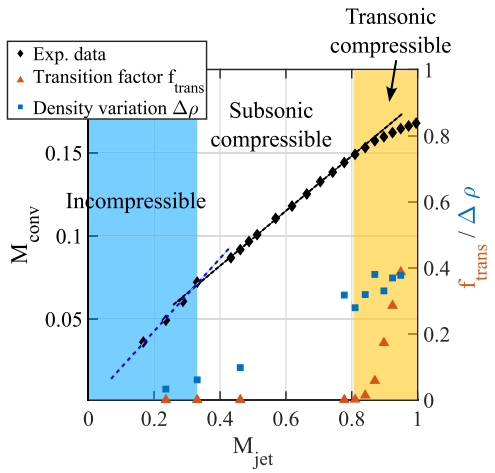

Fig. 10. Summary of the different regime inside the SWJ actuator. Evolution of both coefficients use to define the three regimes.

the transonic transition inside the SWJ and the transition from incompressible regime to compressible regime, computational fluid dynamic simulations are performed using the Fluent solver (ANSYS). 2D mesh and URANS turbulence modelling with the k-epsilon RNG model are used. The structured mesh used is composed of 326 000 cells and the time step is set at 10^{-6} s. Several inlet pressure are tested in the transonic transition region ($50 \leq P_0 \leq 80$ kPa) and at the compressible regime transition ($P_0 = 4; 8; 16$ kPa). To assess the transonic aspect of the flow, a transition factor is defined as:

$$f_{trans} = N_{M>1}/N_{tot} \tag{4}$$

where $N_{M>1}$ corresponds at the number of acquisition point at supersonic speed inside the SWJ, and N_{tot} the total number of acquisition point. Therefore, the flow is transonic when $f_{trans} > 0$. Then, compressibility of the flow is defined with the variation of the density inside the SWJ.

$$\Delta\rho = \frac{\rho_{max} - \rho_{min}}{\rho_{max}} \tag{5}$$

The subscript max and min are for the maximum and the minimum values of the density inside the SWJ. Hence, the flow is considered compressible when $\Delta\rho \geq 0.05$.

Fig. 10 presents the evolution of both coefficient for all simulated cases. The transition factor differs from zero for $M_{jet} \geq 0.8$, which confirms the transonic transition for an inlet pressure $P_0 \geq 50$ kPa (orange zone). In the same way, the density variation shows compressible flow for inlet pressure $P_0 \geq 10$ kPa (blue zone). Despite those changes in the geometry of the jet, the symmetry of the outflow produced by the sweeping jet remains fairly constant as shown in Fig. 9c. For all of the pressure tested in this study, the shape coefficient is really close to 1. The left part of the jet is also slightly flatter than the right part with $F_L \sim 1.5$ and $F_R \sim 1.65$.

Spectral triple decomposition. As the jet is fully turbulent, the objective here is to extract the coherent and incoherent structures of the jet based on a Reynolds decomposition. Here, a triple decomposition method is used, in order to separate the velocity u into three components: the mean velocity U, the coherent fluctuation $\tilde{u}$ and the turbulent fluctuation u':

$$u = U + \tilde{u} + u' \tag{6}$$

where, the coherent fluctuation is estimated using a phase averaging (denoted with $\langle\bullet\rangle$) with $\tilde{u} = \langle u\rangle - U$, and the turbulent fluctuation is the residue ($u' = u - \langle u\rangle$) (Hussain and Reynolds [51]). This method implies the use of phase averaging. Thus hot-wire signals need to be

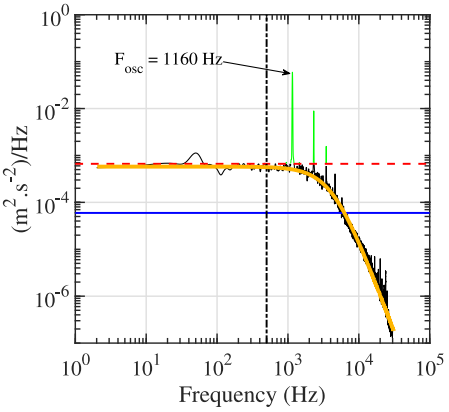

Fig. 11. Methodology for the triple decomposition. (——) Turbulent part of the spectrum. (——) Oscillation part of the signal. (——) 0.01% of the maximum peak. (– –) Low limit cut-off for the decomposition. (– –) Low frequency limit for the application of the algorithm. (——) Approximation of the turbulent part of the signal using Bullen estimation.

synchronised using a reference signal. Which is not suitable with our HWA measurements since no reference signals are taken during the experiment.

An alternative is therefore proposed in the present work. It is based on a decomposition of the variance of the signal into a coherent variance (due to oscillations) and an incoherent one (due to turbulence). From Eq. (6), the variance $\sigma(u)^2$ of the instantaneous velocity is estimated as:

$$\sigma(u)^2 = \sigma_{osc}(u)^2 + \sigma_{turb}(u)^2 \tag{7}$$

Generally, the standard deviation of a signal can be calculated using the Parseval's theorem:

$$\int_{-\infty}^{+\infty} |u(t)|^2 dt = \int_{-\infty}^{+\infty} S(f) df \tag{8}$$

Eq. (8) shows an equivalence between the mean square of a signal (the variance) and the integral of its power spectral density $S(f)$. Besides, the spectrum of a velocity signal is symmetric, leading to:

$$\sigma(u)^2 = 2\int_{0}^{+\infty} S(f) df \tag{9}$$

We now need to estimate the incoherent part of the spectrum in order to calculate $\sigma_{turb}(u)^2$. To do so, the coherent part of the spectrum is extracted. The methodology to extract the coherent signal is presented in Fig. 11. A threshold representing 99.9% of the energy contained in the highest peak of the oscillation frequency is chosen. This decomposition is only applied on high frequency in order to preserve the low-frequency part of the spectrum (below $f_{cut} = 500$ Hz). A lower-limit is also defined as the highest peak of the turbulent signal in the interest zone, to clearly remove part of the turbulent signal. The coherent part of the spectrum S_{osc} is then extracted (Fig. 11, green line).

In the next step, the remaining signal (black curve on Fig. 11) is approximated with a theoretical turbulent spectrum (orange curve). The theoretical spectrum chosen in our study is the Bullen spectrum, corresponding to an isotropic and homogeneous turbulence spectrum models [52].

This spectrum depends on three parameters: the integral length scale $\mathcal{L}$, the constant n defining the slope of the spectrum at high frequencies and v_0 a model constant.

Therefore, the turbulent part of the standard deviation is estimated using Eq. (10) and the oscillating part using Eq. (7).

$$\sigma_{turb}(u)^2 = 2\int_{0}^{+\infty} S_{Bullen}(f) df \tag{10}$$

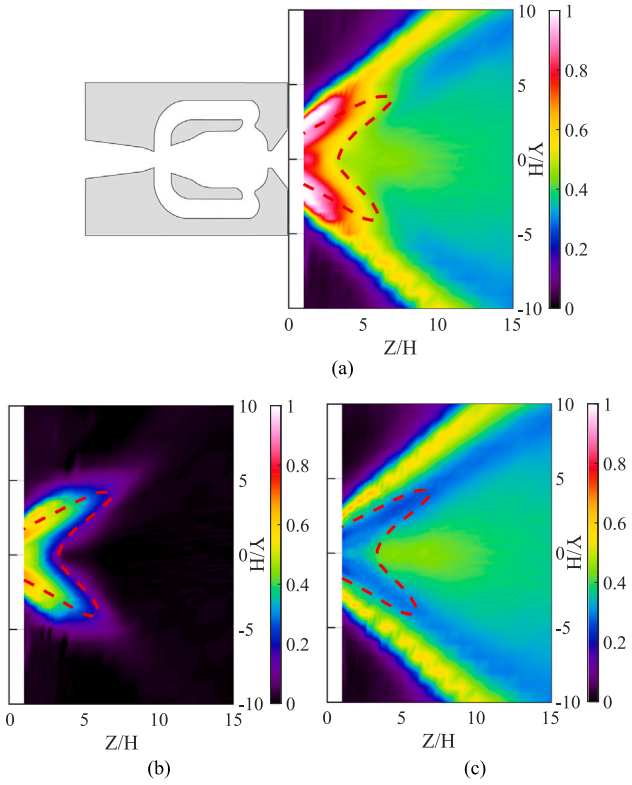

Fig. 12. Decomposition of the intensity of fluctuation field for $P_0 = 20$ kPa. (a) Classic standard deviation $\sigma(u)/U$, (b) the oscillating intensity $I_{osc} = \sigma_{osc}(u)/U$, (c) the turbulence intensity $I_{turb} = \sigma_{turb}(u)/U$. (– –) defined previously.

Results of this decomposition are presented in Fig. 12 for an inlet pressure $P_0 = 20$ kPa. The three extracted components are included: the standard deviation of the signal (Fig. 12a), the oscillating part (Fig. 12b) and the turbulent part (Fig. 12c). As shown in Fig. 12b, the oscillating intensity contributes for the main part to the total fluctuating intensity close the actuator. It means fluctuations are dominated by the oscillatory motion close to the jet exit, then the flow is dominated by incoherent structures away from the jet exit.

The turbulence created by the jet can be separated in three distinct zones, visible in Fig. 12c.

(i) The switching zone is first identifiable as the top centre of the map ($Z/H > 5$ and $|Y/H| < 5$), corresponding to the passing zone of the jet during the switching mechanism. In that region, the variance and the turbulence are moderate (around $0.5U$), where the oscillating part is negligible. This turbulent region is created fairly close to the jet outlet, at approximately $\approx 8H$.

(ii) The jet zone can also be observed in oblique directions (corresponding to the jet angle). Contrary to the first zone, the turbulence intensity is the lowest when the mean velocity is important. This region is dominated by coherent fluctuations, corresponding to the main residence positions of the jets. In this region the flow is the same as the one produced by a turbulent round jet with the same turbulence intensity at about 0.2 U (see reference book of Pope [53]).

(iii) Further is the shear layer region, corresponding to a turbulence level at the highest value compared to the two previous zones. Compared to zone (ii), it is also generated when the jet stays at its residency positions. In this region the mixing produce by the jet is strong and it begins close to the jet outlet and continues away downstream. Each zone is characterised by a different dynamics. Spectral analysis is therefore presented in Fig. 13 for two inlet pressures ($P_0 = 20$ kPa and 100 kPa). The switching zone is defined by a dominant peak, corresponding to twice the oscillatory mechanism frequency ($2f_{osc}$).

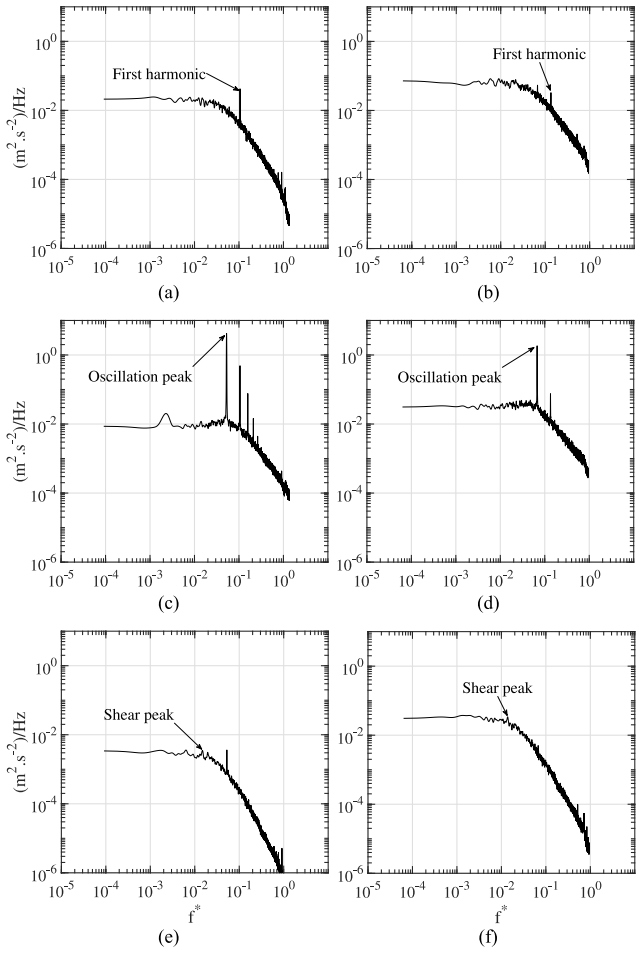

Fig. 13. Spectra of signals in the three different zones. Columns from left to right: P0 = 20 kPa and 100 kPa. Lines from top to bottom: switching zone (a) and (b), jet zone (c) and (d), shear zone (e) and (f). With the normalised frequency $f^* = \frac{fH}{U_{ref}}$.

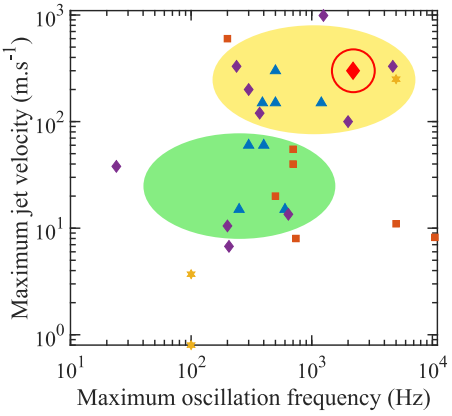

Fig. 14. Placement of the SWJ in the literature. The legend is the same as Fig. 2 and the current work is represented with the red diamond.

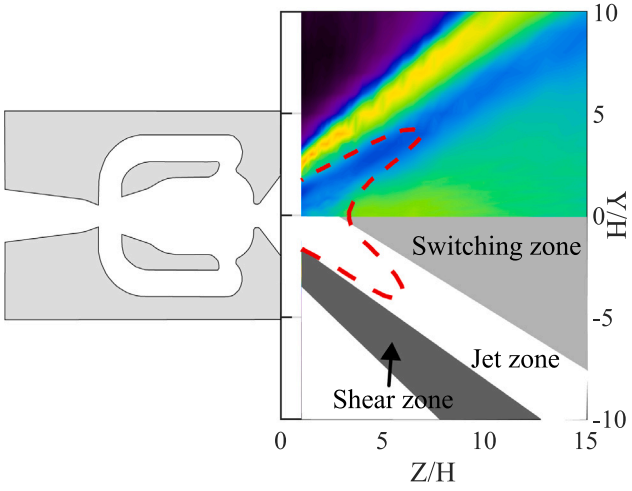

Fig. 15. Illustration of the different zones. (- -) corresponds to the jet threshold define at the beginning of this work.

This is particularly well illustrated for the 20 kPa case where only this frequency is visible in the spectrum. The produced jet passes in this region twice during an oscillatory period, leading logically to this peak at $2f_{osc}$. The jet zone is mostly defined by the oscillatory frequency (Fig. 13b). The harmonics are particularly visible as this oscillation largely dominates the region. For the inlet pressure presented here, it matches well the oscillation frequencies shown in Fig. 6. The last region corresponding to the shear layer shows a short peak at $f^* = 0.014$ (Fig. 13e and f). This peak is not associated with the oscillation mechanism and corresponds to a frequency of between 300 Hz and 450 Hz (respectively for $P_0 = 20$ kPa and $P_0 = 100$ kPa).

4. Conclusion and perspectives

In this study, the flow produced by the SWJ has been characterised. First, in terms of dynamics by observing the oscillation frequency of the latter. It is found that the dynamic of the sweeping jet is highly dependent on the geometry of the latter. Particularly the throat-to-throat distance L_{osc}. The compressibility of the flow also has an important impact on the oscillation frequency of the sweeping, which reaches its maximum frequency when the jet becomes sonic. It is shown that the SWJ is able to produce high momentum with an outlet velocity peaks at up to 300 m s^{-1}. According to Fig. 14, SWJs are the perfectly suitable for aeronautic applications.

The geometry of the flow is studied. It is found that the shape of the mean flow produced by the sweeping jet is influenced by the internal switching mechanism. Knowing the residence time of the flow inside the actuator for each step of the oscillation, it could be possible to estimate the general shape of the produced flow. During this work, the flow inside the actuator goes through a transonic phase $M_{jet} \geq 0.8$. The transition between the subsonic and transonic regimes has an important influence on the evolution of the geometry of the produced flow. The evolution of the height and width of the jet changes during the transition. For high pressure, a maximum width is found and will be used as a minimum spacing between two actuators for control applications. The jet angle α is also influenced. Before the transition, the jet angle increases from 60° to 70°, and then, after the transition, it decreases to reach 60°. Despite those changes, the jet remains symmetric for all tested pressures.

Finally, the turbulence produced by the SWJ is studied. During the experiment, since no reference signal is taken, the classic triple decomposition is not suitable to extract the incoherent fluctuations produced by the SWJ. Thus, a spectral approach to the triple decomposition is proposed. This way, the turbulent intensity is extracted from the hot-wire signals. Three different zones of turbulence, where the physics of the produced jet differs, are created by the jet. Each zone has its own specificity and is recapitulated in Fig. 15. Two zones, the switching zone and the shear zone, are characterised by a high turbulent intensity. The last zone (jet zone) presents a lower turbulent intensity comparable to the one found in the centre line of a turbulent round jet.

As presented above, the geometry of the produced flow is influenced by a transonic transition inside the SWJ. However, the internal mach number is estimated using isentropic calculation in this study. Thus, future work is needed to clearly identify, at least qualitatively, this transition and its impact. Based on previous work in the team using Schlieren visualisation on injectors, a transparent SWJ will be made to study the internal flow using Schlieren visualisation, similar to Hirsh and Gharib [37]. Those measurements could also be used to visualise the internal mechanism and to clearly correlate the inside residence time with the shape of the produced flow.

The SWJ is developed for control purposes, meaning that several actuators will be used in the same configuration. For high inlet pressure, the width of the produced flow w reaches a maximum of 14H, suggesting that for practical applications of these actuators for flow control, two side-by-side sweeping jets need to be 14H spaced apart. The length of the jet is an important parameter as well. In the current study, the length of produced flow is for the highest inlet pressure equal to 13H, which corresponds to ≈30 mm. It is of the same order of magnitude as the incoming boundary layer found in flows over a descending ramp [54,55]. That way, the momentum injection induced by the SWJ will be mainly focused inside the boundary layer in order to be energised. The SWJ jet also produced two turbulent zones: the mixing zone and the shear zone. In flow control applications, they can be generated inside the incoming boundary layer. Creating a high mixing zone inside the latter which will be energised in order to mitigate turbulent separations.

CRediT authorship contribution statement

Mathieu Tocquer: Writing – original draft, Experimental acquisition, Validation, Methodology, Investigation, Formal analysis, Data curation, Conceptualization. **Cédric Raibaudo:** Writing – review & editing, Validation, Supervision, Project administration. **Azeddine Kourta:** Writing – review & editing, Validation, Supervision, Resources, Project administration, Funding acquisition.

Declaration of competing interest

The authors declare that they have no known competing financial interests or personal relationships that could have appeared to influence the work reported in this paper.

Data availability

Data will be made available on request.

Acknowledgements

We would like to gratefully acknowledge the laboratory of Excellence CAPRYSSES framework and the financial support of this study from Grant No. ANR-11-LABX-0006-01 of the Investissements d'Avenir LabEx CAPRYSSES. We would also like to thank Stéphane Loyer for his help during the experiments and Pierre-Yves Passaggia for his advises during the post-processing.

Appendix. Scaling of oscillation frequency

In 2015, Von Gosen et al. [56] showed a correlation between the exit Mach number and the oscillation frequency. Later, Schmidt et al. [35] proposed to scale the oscillation frequency, in term of convective velocity U_{conv} (see Eq. (A.1)), and by plotting the latter against the exit jet velocity, they showed a linear correlation where different sweeping jet geometries, scales and operating fluids collapsed. In their study, they only studied incompressible flow regime. The convective velocity can be interpreted as the mean velocity inside the feedback loops of the sweeping jet actuator.

$$U_{conv} = 2.f_{osc}.L_{osc} \tag{A.1}$$

In 2018, Hirsch and Gharib [37] compared the linear trend proposed by Schmidt et al. [35] with their results on other sweeping jet geometries and at compressible flow regimes. They suggested a new trend between the convective mach number and the exit Mach number (Eqs. (A.2) and (A.3)). Where the exit Mach number at the outlet throat is estimated using isentropic laws.

$$M_{conv} = \frac{2.f_{osc}.L_{osc}}{a} = \frac{U_{conv}}{a} \tag{A.2}$$

$$M_{jet} = \sqrt{\frac{2}{\gamma - 1}\left[\left(\frac{P_\infty}{P_0}\right)^{-\frac{\gamma-1}{\gamma}} - 1\right]} \tag{A.3}$$

References

[1] O.A. Guide, How much fuel does a plane use during flight? 2024, https://www.oag.com/blog/which-part-flight-uses-most-fuel (Accessed 11 March 2024).
[2] M. Serdar Genç, K. Koca, H.H. Açikel, Investigation of pre-stall flow control on wind turbine blade airfoil using roughness element, Energy 176 (2019) 320–334, http://dx.doi.org/10.1016/j.energy.2019.03.179.
[3] G. Godard, M. Stanislas, Control of a decelerating boundary layer. Part 1: Optimization of passive vortex generators, Aerosp. Sci. Technol. 10 (3) (2006) 181–191, http://dx.doi.org/10.1016/j.ast.2005.11.007.
[4] S. Aubrun, J. McNally, F. Alvi, A. Kourta, Separation flow control on a generic ground vehicle using steady microjet arrays, Exp. Fluids 51 (5) (2011) 1177–1187, http://dx.doi.org/10.1007/s00348-011-1132-0.
[5] C. Raibaudo, M. Stanislas, F. Kerhervé, Transient characterization of the reattachment of a massively separated turbulent boundary layer under flow control, Flow Turbul. Combust. 98 (4) (2017) 1039–1063, http://dx.doi.org/10.1007/s10494-016-9796-4.
[6] M. Amitay, B. Smith, A. Glezer, Aerodynamic flow control using synthetic jet technology, in: 36th AIAA Aerospace Sciences Meeting and Exhibit, American Institute of Aeronautics and Astronautics, Reno,NV,U.S.A., 1998, http://dx.doi.org/10.2514/6.1998-208.
[7] A. Glezer, Some aspects of aerodynamic flow control using synthetic-jet actuation, Phil. Trans. R. Soc. A 369 (1940) (2011) 1476–1494, http://dx.doi.org/10.1098/rsta.2010.0374.
[8] A. Kourta, C. Leclerc, Characterization of synthetic jet actuation with application to Ahmed body wake, Sensors Actuators A 192 (2013) 13–26, http://dx.doi.org/10.1016/j.sna.2012.12.008.
[9] S. Wang, L. Baldas, S. Colin, S. Orieux, A. Kourta, N. Mazellier, Experimental and numerical study of the frequency response of a fluidic oscillator for active flow control, in: 8th AIAA Flow Control Conference, American Institute of Aeronautics and Astronautics, Washington, D.C., 2016, http://dx.doi.org/10.2514/6.2016-4234.
[10] T.C. Corke, C.L. Enloe, S.P. Wilkinson, Dielectric barrier discharge plasma actuators for flow control, Annu. Rev. Fluid Mech. 42 (1) (2010) 505–529, http://dx.doi.org/10.1146/annurev-fluid-121108-145550.
[11] L.N. Cattafesta, M. Sheplak, Actuators for active flow control, Annu. Rev. Fluid Mech. 43 (1) (2011) 247–272, http://dx.doi.org/10.1146/annurev-fluid-122109-160634.
[12] J.-R. Frutos, D. Vernier, F. Bastien, M. de Labachelerie, Y. Bailly, An electrostatically actuated valve for turbulent boundary layer control, in: IEEE Sensors, 2005., IEEE, Irvine, CA, USA, 2005, pp. 82–88, http://dx.doi.org/10.1109/ICSENS.2005.1597642.
[13] O. Ducloux, R. Viard, A. Talbi, L. Gimeno, Y. Deblock, P. Pernod, V. Preobrazhensky, A. Merlen, A magnetically actuated, high momentum rate MEMS pulsed microjet for active flow control, J. Micromech. Microeng. 19 (11) (2009) 115031, http://dx.doi.org/10.1088/0960-1317/19/11/115031.
[14] R. Viard, A. Talbi, P. Pernod, V. Preobrazhensky, A. Merlen, Magnetostatic microvalve for high momentum rate pulsed jet generation, Procedia Chem. 1 (1) (2009) 421–424, http://dx.doi.org/10.1016/j.proche.2009.07.105.
[15] P. Pernod, V. Preobrazhensky, A. Merlen, O. Ducloux, A. Talbi, L. Gimeno, R. Viard, N. Tiercelin, MEMS magneto-mechanical microvalves (MMMS) for aerodynamic active flow control, J. Magn. Magn. Mater. 322 (9–12) (2010) 1642–1646, http://dx.doi.org/10.1016/j.jmmm.2009.04.086.
[16] C. Warsop, M. Hucker, A.J. Press, P. Dawson, Pulsed air-jet actuators for flow separation control, Flow Turbul. Combust. 78 (3–4) (2007) 255–281, http://dx.doi.org/10.1007/s10494-006-9060-4.
[17] P. Joseph, X. Amandolèse, J.-L. Aider, Drag reduction on the 25° slant angle Ahmed reference body using pulsed jets, Exp. Fluids 52 (5) (2012) 1169–1185, http://dx.doi.org/10.1007/s00348-011-1245-5.

[18] P. Joseph, X. Amandolese, C. Edouard, J.-L. Aider, Flow control using MEMS pulsed micro-jets on the Ahmed body, Exp. Fluids 54 (1) (2013) 1442, http://dx.doi.org/10.1007/s00348-012-1442-x.
[19] D. Barros, T. Ruiz, J. Borée, B. Noack, Control of a three-dimensional blunt body wake using low and high frequency pulsed jets, in: S. Krajnovic (Ed.), Int. J. Flow Control 6 (1) (2014) 61–74, http://dx.doi.org/10.1260/1756-8250.6.1.61.
[20] L. Gimeno, A. Talbi, R. Viard, A. Merlen, P. Pernod, V. Preobrazhensky, Synthetic jets based on micro magneto mechanical systems for aerodynamic flow control, J. Micromech. Microeng. 20 (7) (2010) 075004, http://dx.doi.org/10.1088/0960-1317/20/7/075004.
[21] S. Wang, B. Ma, J. Deng, H. Qu, J. Luo, Fabrication and characterization of MEMS piezoelectric synthetic jet actuators with bulk-micromachined PZT thick film, Microsyst. Technol. 21 (5) (2015) 1053–1059, http://dx.doi.org/10.1007/s00542-014-2278-5.
[22] T.M. Crittenden, A. Glezer, A high-speed, compressible synthetic jet, Phys. Fluids 18 (1) (2006) 017107, http://dx.doi.org/10.1063/1.2166451.
[23] J. Deng, W. Yuan, J. Luo, D. Shen, B. Ma, Design and fabrication of a piezoelectric micro synthetic jet actuator, in: 2011 6th IEEE International Conference on Nano/Micro Engineered and Molecular Systems, IEEE, Kaohsiung, Taiwan, 2011, pp. 301–304, http://dx.doi.org/10.1109/NEMS.2011.6017353.
[24] J.-C. Gerbedoen, A. Talbi, R. Viard, V. Preobrazhensky, A. Merlen, P. Pernod, Joint International Laboratory LIA LICS, Elaboration of compact synthetic micro-jets based on micro magneto-mechanical systems for aerodynamic flow control, Procedia Eng. 120 (2015) 740–743, http://dx.doi.org/10.1016/j.proeng.2015.08.789.
[25] A. Santhanakrishnan, J.D. Jacob, Flow control with plasma synthetic jet actuators, J. Phys. D: Appl. Phys. 40 (3) (2007) 637–651, http://dx.doi.org/10.1088/0022-3727/40/3/S02.
[26] V. Boucinha, R. Weber, A. Kourta, Drag reduction of a 3D bluff body using plasma actuators, Int. J. Aerodyn. 1 (3/4) (2011) 262, http://dx.doi.org/10.1504/IJAD.2011.038845.
[27] V. Narayanaswamy, L.L. Raja, N.T. Clemens, Characterization of a high-frequency pulsed-plasma jet actuator for supersonic flow control, AIAA J. 48 (2) (2010) 297–305, http://dx.doi.org/10.2514/1.41352.
[28] O. Ducloux, A. Talbi, L. Gimeno, R. Viard, P. Pernod, V. Preobrazhensky, A. Merlen, Self-oscillation mode due to fluid-structure interaction in a micromechanical valve, Appl. Phys. Lett. 91 (3) (2007) 034101, http://dx.doi.org/10.1063/1.2752530.
[29] S. Wang, A. Batikh, L. Baldas, A. Kourta, N. Mazellier, S. Colin, S. Orieux, On the modelling of the switching mechanisms of a Coanda fluidic oscillator, Sensors Actuators A 299 (2019) 111618, http://dx.doi.org/10.1016/j.sna.2019.111618.
[30] F. Ostermann, R. Woszidlo, C.N. Nayeri, C.O. Paschereit, Properties of a sweeping jet emitted from a fluidic oscillator, J. Fluid Mech. 857 (2018) 216–238, http://dx.doi.org/10.1017/jfm.2018.739.
[31] R. Woszidlo, H. Nawroth, S. Raghu, I. Wygnanski, Parametric study of sweeping jet actuators for separation control, in: 5th Flow Control Conference, American Institute of Aeronautics and Astronautics, Illinois, 2012, http://dx.doi.org/10.2514/6.2010-4247.
[32] R.E. Childs, P.M. Stremel, L.K. Kushner, J.T. Heineck, B.L. Storms, Simulation of sweep-jet flow control, single jet and full vertical tail, in: 54th AIAA Aerospace Sciences Meeting, American Institute of Aeronautics and Astronautics, San Diego, California, USA, 2016, http://dx.doi.org/10.2514/6.2016-0569.
[33] D. Veerasamy, A.R. Tajik, L. Pastur, V. Parezanović, Effect of base blowing by a large-scale fluidic oscillator on the bistable wake behind a flat-back Ahmed body, Phys. Fluids 34 (3) (2022) 035115, http://dx.doi.org/10.1063/5.0082844.
[34] T.I. Khan, A.R. Tajik, V. Parezanovic, Drag reduction of a generic transport vehicle model using a fluidic oscillator, Int. J. Thermofluids 15 (2022) 100180, http://dx.doi.org/10.1016/j.ijft.2022.100180.
[35] H.J. Schmidt, R. Woszidlo, C.N. Nayeri, C.O. Paschereit, Separation control with fluidic oscillators in water, Exp. Fluids 58 (8) (2017) 106, http://dx.doi.org/10.1007/s00348-017-2392-0.
[36] M. Koklu, L.G. Pack Melton, Sweeping jet actuator in a quiescent environment, in: 43rd Fluid Dynamics Conference, American Institute of Aeronautics and Astronautics, San Diego, CA, 2013, http://dx.doi.org/10.2514/6.2013-2477.
[37] D. Hirsch, M. Gharib, Schlieren visualization and analysis of sweeping jet actuator dynamics, AIAA J. 56 (8) (2018) 2947–2960, http://dx.doi.org/10.2514/1.J056776.
[38] H.C. Bray, Cold weather fluidic fan spray, 1984.
[39] R.D. Stouffer, Liquid oscillator device, 1985.
[40] G. Raman, S. Raghu, Cavity resonance suppression using miniature fluidic oscillators, AIAA J. 42 (12) (2004) 2608–2612, http://dx.doi.org/10.2514/1.521.
[41] R. Woszidlo, I. Wygnanski, Parameters Governing Separation Control with Sweeping Jet Actuators (Ph.D. thesis), American Institute of Aeronautics and Astronautics, Honolulu, Hawaii, 2011.
[42] M.Y. Andino, J.C. Lin, A.E. Washburn, E.A. Whalen, E.C. Graff, I.J. Wygnanski, Flow separation control on a full-scale vertical tail model using sweeping jet actuators, in: 53rd AIAA Aerospace Sciences Meeting, American Institute of Aeronautics and Astronautics, Kissimmee, Florida, 2015, http://dx.doi.org/10.2514/6.2015-0785.
[43] A.R. Tajik, K. Kara, V. Parezanović, Sensitivity of a fluidic oscillator to modifications of feedback channel and mixing chamber geometry, Exp. Fluids 62 (12) (2021) 250, http://dx.doi.org/10.1007/s00348-021-03342-0.
[44] M. Tocquer, C. Raibaudo, A. Kourta, 58th 3AF International Conference on Applied Aerodynamics, Association Aéronautique et Astronautique de France, Orléans, France, 2024.
[45] H.H. Bruun, Hot-wire anemometry: Principles and signal analysis, Meas. Sci. Technol. 7 (10) (1996) 024, http://dx.doi.org/10.1088/0957-0233/7/10/024.
[46] Y. Peng, X. Zhu, F. Nie, W. Kong, Y. Ge, Fuzzy graph clustering, Inform. Sci. 571 (2021) 38–49, http://dx.doi.org/10.1016/j.ins.2021.04.058.
[47] M. Versaci, G. Angiulli, P. Crucitti, D. De Carlo, F. Laganà, D. Pellicanò, A. Palumbo, A fuzzy similarity-based approach to classify numerically simulated and experimentally detected carbon fiber-reinforced polymer plate defects, Sensors 22 (11) (2022) 4232, http://dx.doi.org/10.3390/s22114232.
[48] J.-X. Wang, H. Xiao, Data-driven CFD modeling of turbulent flows through complex structures, Int. J. Heat Fluid Flow 62 (2016) 138–149, http://dx.doi.org/10.1016/j.ijheatfluidflow.2016.11.007.
[49] W.N. Edeling, G. Iaccarino, P. Cinnella, Data-free and data-driven rans predictions with quantified uncertainty, Flow Turbul. Combust. 100 (3) (2018) 593–616, http://dx.doi.org/10.1007/s10494-017-9870-6.
[50] A.R. Tajik, T.I. Khan, V. Parezanović, Raster angle impact on FDM-based additive manufactured fluidic oscillator, Int. J. Thermofluids 16 (2022) 100230, http://dx.doi.org/10.1016/j.ijft.2022.100230.
[51] A.K.M.F. Hussain, W.C. Reynolds, The mechanics of an organized wave in turbulent shear flow, J. Fluid Mech. 41 (2) (1970) 241–258, http://dx.doi.org/10.1017/S0022112070000605.
[52] L. Caldas, C.A. Kissner, M. Behn, U. Tapken, R. Meyer, Comparison of techniques for the estimation of flow parameters of fan inflow turbulence from noisy hot-wire data, in: AIAA AVIATION 2021 FORUM, in: AIAA AVIATION Forum, American Institute of Aeronautics and Astronautics, 2021, http://dx.doi.org/10.2514/6.2021-2487.
[53] S.B. Pope, Turbulent Flows, Cambridge University Press, 2000.
[54] A. Kourta, A. Thacker, R. Joussot, Analysis and characterization of ramp flow separation, Exp. Fluids 56 (5) (2015) 104, http://dx.doi.org/10.1007/s00348-015-1968-9.
[55] F. Stella, N. Mazellier, A. Kourta, Scaling of separated shear layers: an investigation of mass entrainment, J. Fluid Mech. 826 (2017) 851–887, http://dx.doi.org/10.1017/jfm.2017.455.
[56] F. von Gosen, F. Ostermann, R. Woszidlo, C. Nayeri, C.O. Paschereit, Experimental investigation of compressibility effects in a fluidic oscillator, in: 53rd AIAA Aerospace Sciences Meeting, American Institute of Aeronautics and Astronautics, Kissimmee, Florida, 2015, http://dx.doi.org/10.2514/6.2015-0782.

Mathieu Tocquer is an engineer in aerodynamics who graduated from the Ecole Polytech Orléans (France) in September 2021. He begins his Ph.D. in Fluid Mechanics at the PRISME laboratory (Pluridisciplinaire de Recherche en Ingénierie des Systèmes, Mécanique, Energétique) in October 2021. He is doing experimental research. He is currently working on the development of sweeping jet actuators and their characterisation. He is also working on turbulent separation control using fluidic oscillators.

Cédric Raibaudo is an Associate Professor at the University of Orléans, France. He graduated in 2011 from the Ecole Centrale de Lille (France) as a mechanical and fluid dynamics engineer. He received his Ph.D. in Fluid Mechanics from the Ecole Centrale de Lille (France) in 2015. He obtained three postdoctoral fellowships from the University of Calgary (Canada) from 2016 to 2018, then from the ONERA Toulouse (France) from 2018 to 2020, and from the Ecole Centrale de Nantes (France) from 2020 to 2021. His research skills cover large field experimental measurements for fluid mechanics, wakes in environmental flows, reduced order modelling and stochastic methods for model reduction and flow analysis, feedback control and machine learning optimisation for flow modelling and control.

Azeddine Kourta is a Professor at the Polytechnique Engineer School of the University of Orléans since September 2008. Since 1988, he was a Senior Researcher at CNRS and the Head of the EMT2 Group "Ecoulements Monophasiques Transitionnels et Turbulents" (One phase transitional and turbulent flows) at IMFT (Institut de Mécanique des Fluides de Toulouse). He was the head of PRISME laboratory (Pluridisciplinaire de Recherche en Ingénierie des Systèmes, Mécanique, Energétique) from 2012 to 2023. He was the Director of GDR 2502 of CNRS the French network on "Flow Separation Control" from 2002 to 2022. Their area of expertise are active flow control, transition and turbulence, unsteady and compressible flows, aerodynamics and aeroacoustics.